OMNIDIRECTIONAL POLYHEDRAL ULTRASOUND TRANSDUCER FOR POWERING IMPLANTABLE MICRODEVICES

Sayemul Islam[1], Moonchul Park[1], Seung Hyun Song[2], and Albert Kim[1]
[1]Temple University, Philadelphia, Pennsylvania, USA
[2]Sook Myung Women's University, Seoul, Korea

ABSTRACT

Ultrasonic powering is an emerging power source for implantable microdevices due to its superior efficiency in energy transfer at millimeter-scale, long operation distance, and near omnidirectionality. In this paper, we investigate a novel polyhedral ultrasound transducer with emphasis on angular alignment between piezoelectric poling vector and incident waves. Three different polyhedrons (i.e., sphere, octahedron, and dodecahedron) are fabricated via 3D printing lead-free barium titanate ceramic. The maximum output voltage for a unit area occurred at 0° when the poling and waves direction aligned, which were measured to be 0.677±0.071, 1.058±0.049, and 0.709±0.092 V, respectively. At the extreme angular misalignment at 90° (poling and waves perpendicular to each other), only the dodecahedron could sustain the voltage output with 21% reduction, whereas sphere and octahedron dropped by 46%. The results imply that the geometry factor may overcome the poling vector, enabling omnidirectional ultrasonic powering for implantable microdevices.

KEYWORDS

Ultrasonic powering; barium titanate; piezoelectric; omnidirectional; wireless powering; implantable; microdevice.

INTRODUCTION

In modern healthcare, numerous significant implantable devices have led to new insights in continuous monitoring and automated diagnosis for chronic diseases. In some chronic diseases or deficiencies in the natural functions of the organ, implanting multiple sensors and actuators could enable unprecedented management. For example, overactive bladder can be effectively addressed if bladder pressure measurements via implantable pressure sensor or urine volume monitoring via microelectrodes-mediated neural recording are coupled with a sacral neurostimulator [1], [2]. The pacemaker can also precisely control the heart via pH, oxygen, respiration, activity, and drug infusion monitoring [3], [4]. The brain-computer interface with an implantable microelectrode array (where the number of channels can be more than 100) can assist, augment, or repair human cognitive or sensory-motor functions in precise control [5]. However, the long-term and effective operation of such implantable systems requires continuous/frequent supply of energy.

Wireless powering for implantable devices has been heavily researched over the last decade, dating back to the pioneering work of Wen Ko in the 1970s [6] and largely refers to inductive powering. Inductive powering usually exhibits excellent efficiency when the transmitter (TX) and the receiver (RX) coils are similar in size, well-aligned, and separated by a short distance (< 1cm). A commercial example of inductive powering in implantable devices would be a cochlear implant; average power transfer efficiency is 40% when TX and RX coils are 20-29 mm in diameter and are separated by 4-10 mm [7]. However, inductive powering may not provide sufficient power to deeply implantable devices, such as a pacemaker or other implantable devices for cancer therapy (e.g., the microlight source for photodynamic therapy [8] and in-situ cisplatin synthesis microdevice for regional chemotherapy [9]).

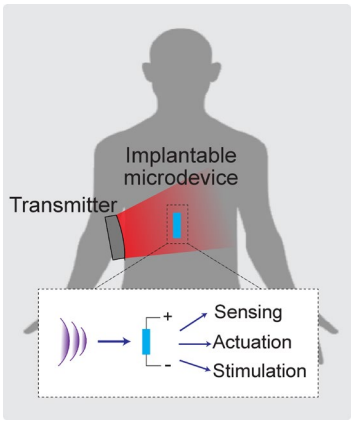

Figure 1: Ultrasonic powering for an implantable microdevice: a portion of ultrasonic waves from a transmitter can be captured by a piezoelectric receiver, which converts it into electrical power. The converted electrical energy can power various implantable devices for sensing, actuation, stimulation or others.

Ultrasonic powering is also a very well-researched technology and has been widely used in various clinical imaging applications [10], and more recently, in power transfer [11]. Figure 1 illustrates the concept of ultrasonic powering for implantable devices. Ultrasonic waves at 1 – 10 MHz frequency range propagates through the body. A deeply seated microdevice can pick up the portion of ultrasonic waves and convert them into electrical power via a piezoelectric receiver. This electrical power can operate various life-sustaining functions, including but not limited to sensing, actuation, drug delivery, stimulation. Ultrasonic powering offers overarching advantages of long-distance operation, high efficiency with the mm-scale receiver, and most importantly, omnidirectionality. Previously, researchers reported that factors contributing to omnidirectionality are RX form factor and reflected waves [12]. Especially, the symmetric cubical RX (e.g., 2×2×2 mm^3) could still generate comparable output power, even if the incident wave was coming in an orthogonal direction to the piezoelectric poling direction (d_{31}) of the RX face. It is because the Poisson ratio compensates for the difference in d_{31} and d_{33} (the poling vector in the same direction as the incident waves). However, even with the cubical RX, true omnidirectional ultrasonic powering could not be achieved at 45°, which is the worst angular misalignment (ultrasonic

waves were facing the edge of RX). Most importantly, the ultrasonic powering still uses lead zirconate titanate (PZT), which raises significant safety concerns due to the lead containment in its composition. In this paper, we report the first demonstration of an omnidirectional, lead-free, 3D printable ultrasonic transducer for powering implantable microdevices using barium titanate (BTO).

DESIGN AND OPERATION

The optimal ultrasonic powering occurs when the incident wave is parallel to the RX face, i.e., the same direction as the poling. However, in reality, the direction of incident waves does not always align with the RX's poling vector. The implanted device may wander through the interstitial space, or the ultrasonic waves may alter due to reflection occurs at different interfaces, such as body/air, fat/muscle, bone/tissue, and others. One possible way to overcome the angular misalignment between transmitting ultrasonic waves and RX's poling direction is increasing the number of RX faces that would parallel to the ultrasonic waves, increasing the probability of the optimal operation. Here, we propose a symmetrical polyhedron, also known as Platonic solid, as an RX; it is constructed by identical shape and size, equal angles and sides, and the same number of faces meeting at each vertex. Figure 2 shows the design of such polyhedral transducers. We utilize octahedron, dodecahedron, and sphere (highest order of polyhedron). The sphere shape RX is expected to provide the most omnidirectional ultrasonic powering since its face would be normal to any incident waves. However, its output voltage is not necessarily the highest because the power output is proportional to poling direction, which is usually reduced in the sphere due to the curved surface. Alternatively, octahedron or dodecahedron shape RX can fulfill both output voltage and omnidirectional ultrasonic powering.

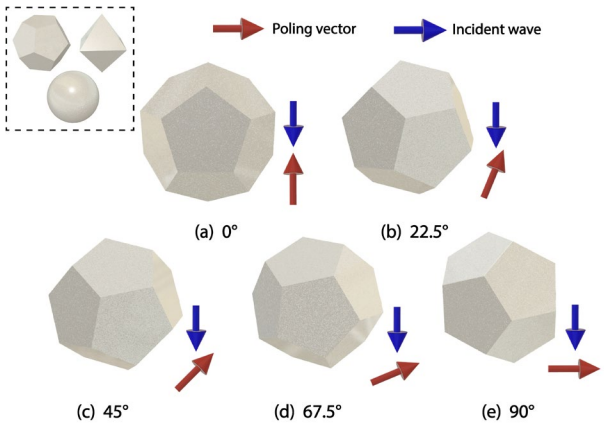

Figure 2: Design of polyhedral ultrasound transducer, showing angular misalignments between the poling vector and incident waves

The polyhedral ultrasound transducer can be fabricated using BTO nanoparticles. BTO is a perovskite crystal, piezoelectric material that has been widely utilized in energy harvesting, ultrasonic transducer, electronic packaging, and electromechanical devices [13], [14]. It is also the material of choice for intravascular ultrasonic transducer for imaging due to its excellent biocompatibility (lead-free). Such BTO is also available as nanoparticles, which can be mixed with an appropriate binding material to create various polyhedral transducers via 3D printing technique and post-processing [15], [16].

MATERIAL AND METHOD

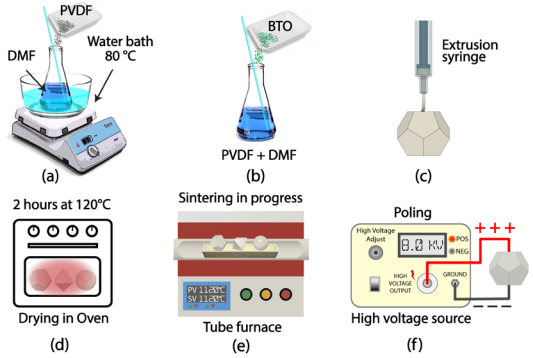

Figure 3: Fabrication procedure involves (a-b) base material preparation, (c) a paste extrusion 3D printing, (d-e) post-processing, and (f) poling

Figure 3 shows the fabrication procedure for the omnidirectional polyhedral ultrasound transducer. To create BTO nanoparticles in a bound state, the base binder was firstly prepared by mixing polyvinyl fluoride (PVDF; Alfa Aesar, USA) in N,N'dimethylformamide (DMF; Thermo Scientific, USA) with 1:8.8 weight ratio at 80 °C water bath for 15 min. The BTO nanoparticles (500 µm; US research nanomaterials, USA) were then slowly introduced to the binder material with continuous stirring until the mixture reached the weight ratio of 3.345:1 for BTO and PVDF/DMF, respectively. After the mixture was thoroughly stirred for an additional 5 min, it was loaded to our custom-made paste extrusion 3d printer; a 10 mL syringe with 600 µm nozzle was used. After printing, octahedron, dodecahedron, and sphere shape transducers were dried at 120 °C for 2 hours in an oven (AccuTemp-09, Across International) to evaporate DMF, which was critical to prevent cracks during the next step.

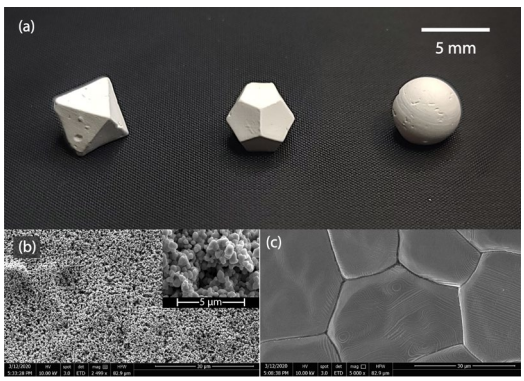

Figure 4: Fabricated polyhedral ultrasound transducer: (a) octahedron, dodecahedron, and sphere, (b) SEM pictures after binding and (c) after sintering

The debinding and sintering processes sequentially occurred in a tubing furnace (GSL 1500X, MTI Corporation, USA). The debinding process was done at 650 °C for 1 hour, followed by the sintering process at

1120 ℃ for 3 hours with a ramp rate of 5 ℃/min. After sintering, randomly oriented ferroelectric domains of the transducers were aligned using custom-made poling stage. The poling stage is equipped with a copper plate at the bottom and a spring-loaded needle electrode from the top. With a built-in heating element in a silicone oil bath, all transducers were poled via a high voltage source (230-30R, Spellman, USA) with an electrical field of 1.0 kV/mm at 120℃ for 1 hour. Figure 4(a) shows a picture of the polyhedral transducer prototype, and Figure 4(b) shows the SEM picture before and after the post-processing. The overall surface areas were equated to 314.1±0.03 mm^2 with the radius of the sphere to be 5 mm, an edge length of 9.5 mm for the octahedron, and 3.9 mm for the dodecahedron.

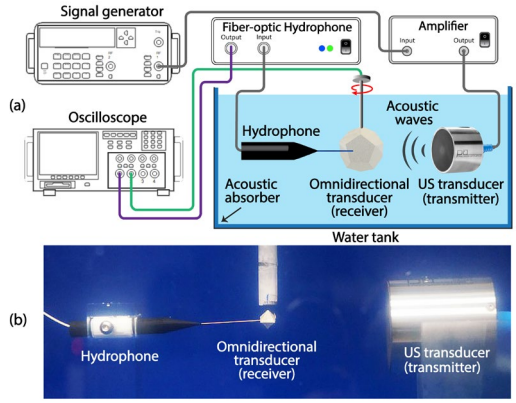

Figure 5: Experimental setup: output voltage and acoustic intensities were measured at the same position

Figure 5 shows an experimental setup. A water tank (60 × 30 × 40 cm^3) with acoustic absorber layers on all sides was used to test the polyhedral ultrasound transducers. For a TX, an immersion planar transducer was used (Precision Acoustics, UK). The transmitter was connected to a function generator (4065, B&K Precision, USA) and an RF amplifier (1040L, E&I, USA). We used fifteen bursts of sinusoidal signals (f = 500 kHz, V = 300 mV_{p-p}). Note that although the resonant frequencies of the transmitter (500 kHz) and receiver (Sphere, Octahedron, and Dodecahedron, 440, 480, and 390 kHz, respectively) were not perfectly matched, the ultrasonic intensity was within 90 % of the matched case. The resonant frequencies of the platonic solid transducers were measured using a network analyzer (E5061B-005, Keysight Tech., USA). To measure the input ultrasonic intensity, a fiber optic hydrophone (FOH64; Precision Acoustics, UK) was positioned next to the polyhedral transducer. Then, the polyhedral transducer was mounted on a manipulator, and the axial angles were rotated up to 180 degrees with a 22.5-degree resolution. The distances between TX and RX in axial and transverse directions were also manipulated. The voltage outputs of the octahedron, dodecahedron, and sphere BTO transducers were measured throughout the rotation using an oscilloscope (MSOX 3024T, Keysight Tech, USA).

RESULTS AND DISCUSSION

Figure 6 shows the output voltage densities (i.e., voltage output per given surface area normal to the incident waves) of sphere, octahedron, and dodecahedron transducers. Note that at least four independent experiments were performed. However, the error bars were omitted for better presentation (it is provided as standard deviation later).

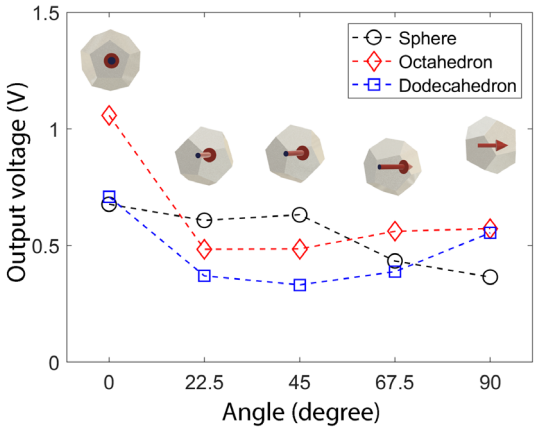

Figure 6: Measured output voltage with respect to the angular alignment

Overall, all transducers showed the highest voltage output per unit area (1 mm^2) at 0°: 1.06±0.049, 0.71±0.092, and 0.68±0.071 V for the octahedron, dodecahedron, and sphere, respectively. At this angle, the incident waves and the poling directions were aligned, i.e., the optimal condition. The voltage outputs were proportional to the surface area of the given projection face normal to the incident wave. For example, the octahedron's larger surface area of 39.3 mm^2 produced higher voltage compared to the dodecahedron (a =26.2 mm^2). In the case of the sphere, despite the largest surface area (78.5 mm^2), its curved area diminished the overall output.

As the transducers were rotated, the sphere exhibited the best omnidirectional behavior, as expected. The measured outputs were 0.68±0.071, 0.61±0.099, 0.63±0.107, 0.43±0.124, and 0.37±0.114 V with the angular alignment of 0°, 22.5°, 45°, 67.5°, and 90°, respectively. The outputs stayed relatively consistent throughout the rotation. However, 67.5° and at 90° showed rapid drop (46 %) due to the poling vector being utterly perpendicular to the incident waves. This result also agrees with the piezoelectric coefficient of BTO; d_{33} = 191 C/N and d_{31} = -79 C/N [17]. It indicates that even with the sphere form factor, the poling property dictates the overall performance than the geometric factor.

The angular misalignment at 45° was the extreme case for both octahedron and dodecahedron since none of the faces were normal to the incident waves, and those vertexes could cause ultrasonic waves scattering. It was more prominent for octahedron; compare to the 0°, the voltage was 0.485±0.188 V, which was >50 % reduction.

The intriguing findings were at 90°, which showed the worst case for the sphere due to perpendicular between poling and incident waves. However, for the octahedron and dodecahedron, the voltage output, in fact, recovered: 0.57±0.189 V for octahedron and 0.55±0.122 V for the dodecahedron. Notably, dodecahedron showed 21.8% reduction, which was significantly lower than that of octahedron (45%) or sphere (46%). Taken together, the

geometric factor of dodecahedron could overcome the poling vector that is usually the dominating factor in most ultrasound transducers.

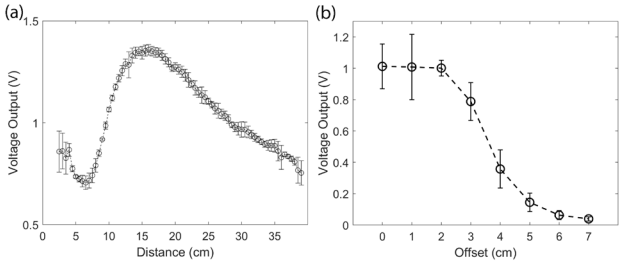

Figure 7: Electrical voltage output vs. (a) axial distance from the TX and (b) transverse distance (offset)

Figure 7 shows the average voltage output of all transducers as a function of (a) axial distance from the TX and (b) transverse distance (offset). As expected, the ultrasonic waves exhibited local minima and maxima and reached the maximum output at the near field distance at approximately 16 cm ($N = D^2/4\lambda$, where N is the onset of far-field distance, D is the transmitter dimension, and λ is the wavelength of the ultrasound in water). While the transducer was fixed at a near-field distance (N = 16 cm), it was also moved in the transverse direction with respect to the one edge of the TX. The voltage output rapidly dropped beyond 3 cm away from the transducer edge.

CONCLUSION

The design, fabrication, and characterization of the sphere, octahedron, and dodecahedron ultrasound transducers were presented. All types of polyhedral transducers exhibited some degree of omnidirectional ultrasonic powering. Among them, the dodecahedron shape could be more suitable for omnidirectional ultrasonic powering than octahedron because vertices with a higher number of faces produced steeper edges, which is the source of ultrasound scattering. Evidently, there was no difference in the voltage output between 0° and 90° for the dodecahedron transducer. However, the surface area normal to the incidence waves was smaller than that of the octahedron, resulting in mediocre output. It is, however, possible to improve by changing the poling direction, which is our future research. In summary, the poling direction was the more dominant factor in the sphere, while polyhedral transducers were more affected by geometric factors, including the surface area, vertex angle, and a number of faces and vertices.

ACKNOWLEDGEMENTS

The authors thank Lucy Arce at Temple University for her help with the experiment. The project was supported by the National Science Foundation (ECCS 2029077).

REFERENCES

[1] T. M. Bruns *et al.*, "Bursting stimulation of proximal urethral afferents improves bladder pressures and," *J. Neural Eng.*, vol. 6, 2009.

[2] C. R. Powell, "Conditional Electrical Stimulation in Animal and Human Models for Neurogenic Bladder : Working Toward a Neuroprosthesis," *Curr. Bladder Dysfunct. Rep.*, vol.11, 2016.

[3] R. G. Hauser, "Techniques for Improving Cardiac Performance with Implantahle Devices," *Pacing Clin. Electrophysiol. PACE*, vol. 7, 1984.

[4] K. Kaszala *et al.*, "Device sensing: Sensors and algorithms for pacemakers and impantable cardioverter defibrillators," *Circulation*, vol. 122, pp. 1328–1340, 2010.

[5] R. A. Normann *et al.*, "Clinical applications of penetrating neural interfaces and Utah Electrode Array technologies," *J. Neural Eng.*, vol. 13, no. 061003, 2016.

[6] W. H. Ko *et al.*, "Design of radio-frequency powered coils for implant instruments," *Med. Biol. Eng. Comput.*, vol. 15, pp. 634–640, 1977.

[7] F. Zeng *et al.*, "Cochlear Implants : System Design , Integration , and Evaluation," *IEEE Rev. Biomed. Eng.*, vol. 1, pp. 115–142, 2008.

[8] A. Kim *et al.*, "An Implantable Ultrasonically-Powered Micro-Light-Source (μ Light) for Photodynamic Therapy," *Sci. Rep.*, vol. 9, no. 1395, pp. 1–9, 2019.

[9] R. Campbell *et al.*, "Implantable Cisplatin Synthesis Microdevice for Regional Chemotherapy," *Adv. Healthc. Mater.*, vol. 10, no. 2001582, pp. 1–7, 2021

[10] K. Agarwal *et al.*, "Wireless Power Transfer Strategies for Impantable Bioelectronics," *IEEE Rev. Biomed. Eng.*, vol. 10, pp. 136–161, 2017.

[11] A. Ibrahim *et al.*, "A Comprehensive Comparative Study on Inductive and Ultrasonic Wireless Power Transmission to Biomedical Implants," *IEEE Sens. J.*, vol. 18, no. 9, pp. 3813–3826, 2018

[12] S. H. Song *et al.*, "Omnidirectional Ultrasonic Powering for Millimeter-Scale Implantable Devices," *IEEE Trans. Biomed. Eng.*, vol. 62, no. 11, pp. 2717–2723, Nov. 2015

[13] J. Yan *et al.*, "High Performance Flexible Piezoelectric Nanogenerators based on BaTiO3 Nano fibers in Different Alignment Modes," *ACS AMI*, vol. 8, pp. 15700–15709, 2016.

[14] H. Elahi *et al.*, "Response of piezoelectric materials on thermomechanical shocking and electrical shocking for aerospace applications," *Microsyst. Technol.*, vol. 24, pp. 3791–3798, 2018.

[15] M. Park *et al.*, "Human Oral Motion-Powered Smart Dental Implant (SDI) for In Situ Ambulatory Photo-biomodulation Therapy," *Adv. Healthc. Mater.*, vol. 9, no. 200658, pp. 1–10, 2020.

[16] H. Kim *et al.*, "Fabrication of bulk piezoelectric and dielectric BaTiO 3 ceramics using paste extrusion 3D printing technique," *J. Am. Ceram. Soc.*, vol. 102, pp. 3685–3694, 2019.

[17] D. Berlincourt *et al.*, "Elastic and Piezoelectric Coefficients of Single-Crystal Barium Titanate," *Phys Rev*, vol. 111, no. 1, pp. 143–148, 1958.

CONTACT

* Prof. Albert Kim, albertkim@temple.edu